Journal of Nonlinear Optical Physics & Materials
Vol. 28, No. 3 (2019) 1950031 (12 pages)

DOI: 10.1142/S0218863519500310

Influence of Doppler broadening on cross-Kerr nonlinearity in a four-level inverted-Y system: An analytical approach

Nguyen Huy Bang*, Dinh Xuan Khoa*, Nguyen Le Thuy An*, Vu Ngoc Sau*, Doan Hoai Son† and Le Van Doai*,‡

*Vinh University, 182 Le Duan Street, Vinh City, Vietnam

†Ha Tinh University, Cam Xuyen District, Ha Tinh Province, Vietnam

‡doailv@vinhuni.edu.vn

Accepted 13 September 2019
Published 16 December 2019

In this work, we study the influence of Doppler broadening on cross-Kerr nonlinearity in a four-level inverted-Y atomic system under electromagnetically induced transparency (EIT) condition. The first- and third-susceptibilities in the presence of Doppler effect are derived as a function of probe, signal and coupling beams and temperature of medium. Under EIT condition, cross-Kerr nonlinearity is enhanced several orders of magnitude compared to that without EIT. The Doppler effect leads to a reduction in the transparent efficiency and thus reduces the amplitude of cross-Kerr nonlinear coefficient. For hot atomic gaseous medium, such consideration of the Doppler effect may be useful for experimental observations and apply to photonic devices operating at different temperature conditions.

Keywords: Electromagnetically induced transparency; Kerr nonlinear effect; Doppler effect.

1. Introduction

The cross-Kerr nonlinearity or the so-called cross-phase modulation (XPM)[1] refers to the phenomenon that the phase of an optical field is modulated by another field, it has received more attention due to its potential important applications in quantum information processing such as quantum phase gate,[2,3] deterministic optical quantum computation,[4] manipulation of quantum information,[5] entanglement of single photons,[6] controlled-NOT (CNOT) gate[7,8] and so on. However, the weakness of Kerr nonlinearity in conventional media becomes an obstacle of its applications in photonic devices. The advent of electromagnetically induced transparency (EIT) delivers media of reduced absorption and giant nonlinearity for a weak probe light.[9]

Using the EIT technique, Schmidt and Imamoglu[10] was first proposed an N-type four-level system to obtain giant cross-Kerr nonlinearity under EIT condition. This

‡Corresponding author.

scheme was experimentally demonstrated in cold Rb atoms by Kang *et al.*[11] Later, Joshi and Xiao[12] found large cross-Kerr nonlinearity in cold Rb four-level inverted-Y atomic system without Doppler effect and can be used for realizing polarization quantum phase gates. Whereas, Xiao *et al.*[13] was first measured the enhanced self-Kerr nonlinear coefficient in three-level Λ-type atomic system of hot Rb atoms. Since then, there are a lot of experimental and theoretical studies in the literature dealing with the enhancement of the Kerr nonlinearity via the EIT effect are proposed.[14–21]

Although experimental observations of Kerr nonlinearity in hot atomic media have been implemented and explained with numerical simulations,[13–17] however, there was still a lack of analytical description of the cross-Kerr nonlinearity. In most applications of nonlinear medium, a precise knowledge of the Kerr nonlinear coefficient as a function of light fields and the temperature of medium is needed to optimize nonlinear optical processes and to study related applications. Recently, we have developed an analytical method to study the Doppler effect on self-Kerr nonlinearity in three-level Λ-type atomic system and compared to experimental results with a good agreement.[20] Such expression of self-Kerr nonlinear coefficient was used to study the control of optical bistability under Doppler effect.[22]

In this paper, we derive the first- and third-susceptibilities for both probe and signal beams and cross-Kerr nonlinear coefficient of four-level inverted-Y atomic system under the Doppler effect. The influences of EIT and Doppler broadening on cross-Kerr nonlinearity are studied. Analytical results of cross-Kerr nonlinearity can apply to related applications in photonic devices operating at different temperatures.

2. Theoretical Model

We consider the interaction of three light fields with a four-level inverted-Y atomic system as shown in Fig. 1. A weak probe laser beam (with frequency ω_p and Rabi frequency Ω_p) applies to the transition $|1\rangle \leftrightarrow |3\rangle$, an intense coupling laser beam (with frequency ω_c and Rabi frequency Ω_c) couples the transition $|3\rangle \leftrightarrow |4\rangle$, and a

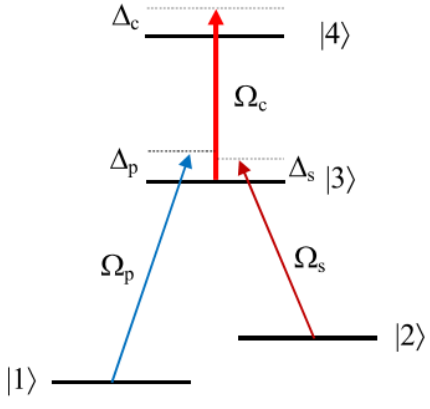

Fig. 1. Four-level inverted-Y atomic system.

weak signal laser beam (with frequency ω_s and Rabi frequency Ω_s) drives the transition $|2\rangle \leftrightarrow |3\rangle$. In this configuration, the coupling beam will produce an EIT effect for the probe beam (and signal beam), while the signal beam will create a cross-Kerr nonlinear effect for the probe beam.

The frequency detuning of the coupling, probe and signal light beams is, respectively, defined as

$$\Delta_c = \omega_c - \omega_{43}, \quad \Delta_p = \omega_p - \omega_{31} \quad \text{and} \quad \Delta_s = \omega_s - \omega_{32}. \tag{1}$$

In the framework of the semiclassical theory, using the dipole and rotating wave approximations, the evolution of system can be represented by the following density matrix equations:

$$\dot{\rho}_{11} = \Gamma_{31}\rho_{33} + i\Omega_p(\rho_{13} - \rho_{31}), \tag{2}$$
$$\dot{\rho}_{22} = -\Gamma_{23}\rho_{22} + i\Omega_s(\rho_{23} - \rho_{32}), \tag{3}$$
$$\dot{\rho}_{33} = -\Gamma_{31}\rho_{33} + \Gamma_{43}\rho_{44} + \Gamma_{23}\rho_{22} + i\Omega_p(\rho_{31} - \rho_{13}) + i\Omega_c(\rho_{34} - \rho_{43}), \tag{4}$$
$$\dot{\rho}_{44} = -\Gamma_{43}\rho_{44} + i\Omega_c(\rho_{43} - \rho_{34}), \tag{5}$$
$$\dot{\rho}_{21} = [i(\Delta_s - \Delta_p) - \gamma_{21}]\rho_{21} + i\Omega_p\rho_{23} - i\Omega_s\rho_{31}, \tag{6}$$
$$\dot{\rho}_{31} = [i\Delta_p - \gamma_{31}]\rho_{31} + i\Omega_p(\rho_{33} - \rho_{11}) - i\Omega_c\rho_{41} - i\Omega_s\rho_{21}, \tag{7}$$
$$\dot{\rho}_{41} = [i(\Delta_c + \Delta_p) - \gamma_{41}]\rho_{41} + i\Omega_p\rho_{43} - i\Omega_c\rho_{31}, \tag{8}$$
$$\dot{\rho}_{23} = [i\Delta_s - \gamma_{32}]\rho_{23} - i\Omega_s(\rho_{33} - \rho_{22}) + i\Omega_P\rho_{21} + i\Omega_c\rho_{24}, \tag{9}$$
$$\dot{\rho}_{24} = [i(\Delta_s - \Delta_c) - \gamma_{42}]\rho_{24} + i\Omega_c\rho_{23} - i\Omega_s\rho_{34}, \tag{10}$$
$$\dot{\rho}_{43} = [i\Delta_c - \gamma_{43}]\rho_{43} + i\Omega_p\rho_{41} + i\Omega_c(\rho_{44} - \rho_{33}), \tag{11}$$
$$\rho_{ki} = \rho_{ik}^*, \tag{12}$$
$$\rho_{11} + \rho_{22} + \rho_{33} + \rho_{44} = 1, \tag{13}$$

where $\Omega_p = 2d_{31}E_p/\hbar$, $\Omega_c = 2d_{42}E_c/\hbar$ and $\Omega_s = 2d_{32}E_s/\hbar$ are Rabi frequency for the probe, coupling and signal fields, respectively; d_{kl} is element of dipole moment of the $|k\rangle - |l\rangle$ transition and γ_{kl} is the decay rate of the atomic coherence ρ_{kl}, given by

$$\gamma_{kl} = \frac{1}{2}\left(\sum_{E_k<E_j}\Gamma_{jk} + \sum_{E_m<E_l}\Gamma_{lm}\right), \tag{14}$$

with, Γ_{kl} is the decay rate of population from level $|k\rangle$ to level $|l\rangle$.

Now, we solve the density-matrix equations under the steady-state condition to find the solutions for density matrix elements related to the probe and signal responses up to third order. Under the assumption that the coupling light intensity Ω_c is much stronger than the probe light intensity Ω_p and signal light intensity Ω_s, therefore from Eqs. (6) and (8) we obtain

$$\rho_{41} = -\frac{i\Omega_c}{\gamma_{41} - i(\Delta_c + \Delta_p)}\rho_{31}, \tag{15}$$

$$\rho_{21} = -\frac{i\Omega_s}{\gamma_{21} - i(\Delta_p - \Delta_s)}\rho_{31} + \frac{i\Omega_p}{\gamma_{21} - i(\Delta_p - \Delta_s)}\rho_{23}. \tag{16}$$

From Eqs. (9)–(11), we find the following relationship:

$$\rho_{23} = -\frac{i\Omega_s(\rho_{33}-\rho_{22})}{\gamma_{32}+i\Delta_s+\frac{\Omega_c^2}{\gamma_{42}+i(\Delta_s+\Delta_c)}} + \frac{i\Omega_P}{\gamma_{32}+i\Delta_s+\frac{\Omega_c^2}{\gamma_{42}+i(\Delta_s+\Delta_c)}}\rho_{21}. \tag{17}$$

By substituting Eq. (17) into Eq. (16) we have

$$\rho_{21} = -\frac{i\Omega_s}{\gamma_{21}-i(\Delta_p-\Delta_s)}\rho_{31} - \frac{\Omega_p\Omega_s(\rho_{22}-\rho_{33})}{\left(\gamma_{21}-i(\Delta_p-\Delta_s)\right)\left(\gamma_{32}+i\Delta_s+\frac{\Omega_c^2}{\gamma_{42}+i(\Delta_s+\Delta_c)}\right)}. \tag{18}$$

Substituting Eqs. (15) and (18) into Eq. (7) we find the solution for density matrix element related to the probe response up to third order as

$$\rho_{31} = -\frac{i\Omega_p(\rho_{11}-\rho_{33})}{A} + \frac{i\Omega_p\Omega_s^2(\rho_{22}-\rho_{33})}{(\gamma_{21}-i(\Delta_p-\Delta_s))A_1A_2}, \tag{19}$$

where

$$A = \gamma_{31} - i\Delta_p + \frac{\Omega_s^2}{\gamma_{21}-i(\Delta_p-\Delta_s)} + \frac{\Omega_c^2}{\gamma_{41}-i(\Delta_p+\Delta_c)}, \tag{20}$$

$$A_1 = \gamma_{32} + i\Delta_s + \frac{\Omega_c^2}{\gamma_{42}+i(\Delta_s+\Delta_c)}, \tag{21}$$

$$A_2 = \gamma_{31} - i\Delta_p + \frac{\Omega_c^2}{\gamma_{41}-i(\Delta_p+\Delta_c)}. \tag{22}$$

Similarly, the solution for density matrix element related to the signal response up to third order is found as

$$\rho_{32} = -\frac{i\Omega_s(\rho_{22}-\rho_{33})}{B} + \frac{i\Omega_s\Omega_p^2(\rho_{11}-\rho_{33})}{(\gamma_{21}+i(\Delta_p-\Delta_s))B_1B_2}, \tag{23}$$

where

$$B = \gamma_{32} - i\Delta_s + \frac{\Omega_p^2}{\gamma_{21}-i(\Delta_p-\Delta_s)} + \frac{\Omega_c^2}{\gamma_{42}-i(\Delta_s+\Delta_c)}, \tag{24}$$

$$B_1 = \gamma_{31} + i\Delta_p + \frac{\Omega_c^2}{\gamma_{41}+i(\Delta_p+\Delta_c)}, \tag{25}$$

$$B_2 = \gamma_{32} - i\Delta_s + \frac{\Omega_c^2}{\gamma_{42}-i(\Delta_s+\Delta_c)}. \tag{26}$$

The total susceptibilities can then be determined by the following relations:

$$\chi_p = -\frac{Nd_{31}}{\varepsilon_0 E_p}\rho_{31} = \frac{iNd_{31}^2}{\varepsilon_0\hbar}\left(\frac{(\rho_{11}-\rho_{33})}{A} - \frac{\Omega_s^2(\rho_{22}-\rho_{33})}{\big(\gamma_{21}-i(\Delta_p-\Delta_s)\big)A_1A_2}\right), \tag{27}$$

$$\chi_s = -\frac{Nd_{32}}{\varepsilon_0 E_s}\rho_{32} = \frac{iNd_{32}^2}{\varepsilon_0\hbar}\left(\frac{(\rho_{22}-\rho_{33})}{B} - \frac{\Omega_p^2(\rho_{11}-\rho_{33})}{\big(\gamma_{21}+i(\Delta_p-\Delta_s)\big)B_1B_2}\right). \tag{28}$$

For hot atoms, it is necessary taken into account Doppler broadening. In order to eliminate the first-order Doppler effect, we consider the signal beam is co-propagating with the probe beam while the coupling beam is counter-propagating with the probe beam in the medium. Therefore, an atom with velocity ν moving towards probe beam will see an up-shift frequency of the probe and signal lasers as $\omega_p + (v/c)\omega_p$ and $\omega_s + (v/c)\omega_s$, and see the down-shift frequency of the coupling beam as $\omega_c - (v/c)\omega_c$. In such case, the frequency detuning of the laser beams are adjusted accordingly as $\Delta_p' = \Delta_p + (v/c)\omega_p$, $\Delta_s' = \Delta_s + (v/c)\omega_s$ and $\Delta_c' = \Delta_c - (v/c)\omega_c$. The numbers of atoms having velocity v which lie along the beams obey a Maxwellian distribution:

$$dN(v) = \frac{N_0}{u\sqrt{\pi}}e^{-v^2/u^2}dv, \tag{29}$$

where $u = \sqrt{2k_BT/m}$, is the root mean square atomic velocity and N_0 is the total atomic density of the atomic medium. So, the susceptibility expressions must be modified to

$$\chi_p(v)dv = \frac{iN_0d_{31}^2}{u\sqrt{\pi}\varepsilon_0\hbar}\left(\frac{(\rho_{11}-\rho_{33})}{A(v)} - \frac{\Omega_s^2(\rho_{22}-\rho_{33})}{\big(\gamma_{21}-i(\Delta_p-\Delta_s)\big)A_1(v)A_2(v)}\right)e^{-v^2/u^2}dv, \tag{30}$$

$$A(v) = \gamma_{31} - i\Big(\Delta_p + \frac{v}{c}\omega_p\Big) + \frac{\Omega_s^2}{\gamma_{21}-i(\Delta_p-\Delta_s)-i\frac{v}{c}(\omega_p-\omega_s)} + \frac{\Omega_c^2}{\gamma_{41}-i(\Delta_p+\Delta_c)-i\frac{v}{c}(\omega_p-\omega_c)}, \tag{31}$$

$$A_1(v) = \gamma_{32} + i\Big(\Delta_s + \frac{v}{c}\omega_s\Big) + \frac{\Omega_c^2}{\gamma_{42}+i(\Delta_s+\Delta_c)+i\frac{v}{c}(\omega_s-\omega_c)}, \tag{32}$$

$$A_2(v) = \gamma_{31} - i\Big(\Delta_p + \frac{v}{c}\omega_p\Big) + \frac{\Omega_c^2}{\gamma_{41}-i(\Delta_p+\Delta_c)-i\frac{v}{c}(\omega_p-\omega_c)}. \tag{33}$$

Since ω_p is close to ω_s and ω_c, so terms $i\frac{v}{c}(\omega_p-\omega_c)$, $i\frac{v}{c}(\omega_s-\omega_c)$ and $i\frac{v}{c}(\omega_p-\omega_s)$ can be neglected, so the expression (30) becomes

$$\chi_p(x)dx = \frac{iN_0d_{32}^2}{u\sqrt{\pi}\varepsilon_0\hbar}\left(\frac{(\rho_{11}-\rho_{33})}{(\omega_p u/c)}\frac{e^{-x^2}}{(a-ix)} - \frac{\Omega_s^2(\rho_{22}-\rho_{33})}{(\gamma_{21}-i(\Delta_p-\Delta_s))(\omega_s u/c)(\omega_p u/c)}\frac{e^{-x^2}}{(a_1+ix)(a_2-ix)}\right)dx, \tag{34}$$

where $x = v/u$ and

$$a = \frac{c}{\omega_p u}\left(\gamma_{31} - i\Delta_p + \frac{\Omega_s^2}{\gamma_{21}-i(\Delta_p-\Delta_s)} + \frac{\Omega_c^2}{\gamma_{41}-i(\Delta_p+\Delta_c)}\right). \tag{35}$$

$$a_1 = \frac{c}{\omega_s u}\left(\gamma_{32} + i\Delta_s + \frac{\Omega_c^2}{\gamma_{42}+i(\Delta_s+\Delta_c)}\right), \tag{36}$$

$$a_2 = \frac{c}{\omega_p u}\left(\gamma_{31} - i\Delta_p + \frac{\Omega_c^2}{\gamma_{41}-i(\Delta_p+\Delta_c)}\right). \tag{37}$$

By integrating the expression (34) over the velocity v from $-\infty$ to $+\infty$, we obtain

$$\chi_p = \frac{iN_0d_{31}^2}{u\sqrt{\pi}\varepsilon_0\hbar}\left(\frac{(\rho_{11}-\rho_{33})}{(\omega_p u/c)}e^{a^2}[1-\mathrm{erf}(a)] - \frac{\Omega_s^2(\rho_{22}-\rho_{33})}{(\gamma_{21}-i(\Delta_p-\Delta_s))}\frac{e^{a_1^2}[1-\mathrm{erf}(a_1)]+e^{a_2^2}[1-\mathrm{erf}(a_2)]}{(\omega_s u/c)(\omega_p u/c)(a_1+a_2)}\right), \tag{38}$$

where erf is error function.

Similarly, the susceptibility for the signal beam under Doppler effect is found as

$$\chi_s = \frac{iN_0d_{32}^2}{u\sqrt{\pi}\varepsilon_0\hbar}\left(\frac{(\rho_{11}-\rho_{33})}{(\omega_s u/c)}e^{b^2}[1-\mathrm{erf}(b)] - \frac{\Omega_p^2(\rho_{22}-\rho_{33})}{(\gamma_{21}+i(\Delta_p-\Delta_s))}\frac{e^{b_1^2}[1-\mathrm{erf}(b_1)]+e^{b_2^2}[1-\mathrm{erf}(b_2)]}{(\omega_p u/c)(\omega_s u/c)(b_1+b_2)}\right), \tag{39}$$

where

$$b = \frac{c}{\omega_p u}\left(\gamma_{32} - i\Delta_s + \frac{\Omega_p^2}{\gamma_{21}-i(\Delta_p-\Delta_s)} + \frac{\Omega_c^2}{\gamma_{42}-i(\Delta_s+\Delta_c)}\right), \tag{40}$$

$$b_1 = \frac{c}{\omega_s u}\left(\gamma_{31} + i\Delta_p + \frac{\Omega_c^2}{\gamma_{41}+i(\Delta_p+\Delta_c)}\right), \tag{41}$$

$$b_2 = \frac{c}{\omega_p u}\left(\gamma_{32} - i\Delta_s + \frac{\Omega_c^2}{\gamma_{42}-i(\Delta_s+\Delta_c)}\right). \tag{42}$$

In order to extract the first- and third-order susceptibilities we can be expressed the susceptibilities for the XMP between probe and signal beams as

$$\chi_p = \chi_p^{(1)} + 3E_s^2\chi_p^{(2)}, \tag{43}$$

$$\chi_s = \chi_s^{(1)} + 3E_p^2\chi_s^{(2)}. \tag{44}$$

Therefore, the expressions for first- and third-order susceptibilities under Doppler effect for the probe light field are determined by

$$\chi_p^{(1)} = \frac{iNd_{31}^2}{\hbar\varepsilon_0}\frac{(\rho_{11}-\rho_{33})}{(\omega_p u/c)}e^{a^2}[1-\mathrm{erf}(a)], \tag{45}$$

$$\chi_p^{(3)} = -\frac{iNd_{31}^2d_{32}^2}{3\hbar^3\varepsilon_0}\frac{(\rho_{22}-\rho_{33})}{(\gamma_{21}-i(\Delta_p-\Delta_s))}\frac{e^{a_1^2}[1-\mathrm{erf}(a_1)]+e^{a_2^2}[1-\mathrm{erf}(a_2)]}{(\omega_s u/c)(\omega_p u/c)(a_1+a_2)}. \tag{46}$$

Similarly, the expressions for first- and third-order susceptibilities under Doppler effect for the signal light field as

$$\chi_s^{(1)} = \frac{iNd_{32}^2}{\hbar\varepsilon_0}\frac{(\rho_{22}-\rho_{33})}{(\omega_s u/c)}e^{b^2}[1-\mathrm{erf}(b)], \tag{47}$$

$$\chi_s^{(3)} = -\frac{iNd_{31}^2d_{32}^2}{3\hbar^3\varepsilon_0}\frac{(\rho_{22}-\rho_{33})}{(\gamma_{21}+i(\Delta_p-\Delta_s))}\frac{e^{b_1^2}[1-\mathrm{erf}(b_1)]+e^{b_2^2}[1-\mathrm{erf}(b_2)]}{(\omega_p u/c)(\omega_s u/c)(b_1+b_2)}. \tag{48}$$

From the first- and third-order susceptibilities, we find the linear dispersion n_0 and cross-Kerr nonlinear n_2 coefficients under Doppler effect for the probe light as[1]:

$$n_0 = 1 + \frac{\mathrm{Re}(\chi_p^{(1)})}{2}, \tag{49}$$

$$n_2 = \frac{3\mathrm{Re}(\chi_p^{(3)})}{2\varepsilon_0 n_0^2 c}. \tag{50}$$

3. Results and Discussion

As a recommendation for an experimental realization of the four-level inverted-Y system, we apply the calculation results to the ^{87}Rb atomic vapor.[23] Two ground levels $|1\rangle$ and $|2\rangle$ are assigned to the states $5S_{1/2}$, $F=1$ and $F=2$, respectively. The states, $|3\rangle$ and $|4\rangle$ are chosen as $5P_{3/2}$, $F'=1$ and $5\,D_{5/2}$, $F''=1$, respectively. The atomic parameters are given by: $N=10^{12}$ atoms/cm^3, $\Gamma_{32}=\Gamma_{42}=\gamma=0.97$ MHz, $\Gamma_{31}=\Gamma_{32}=6$ MHz, $d_{31}=1.6\times10^{-29}$ C.m, $d_{32}=1.6\times10^{-29}$ C.m, $\omega_p=3.77\times10^8$ MHz. For simplicity, all quantities related to frequency are given in units γ.

First of all, in order to see XPM occurring between the probe and signal beams, we plot probe susceptibility χ_p versus probe detuning Δ_p/γ and signal susceptibility χ_s versus signal detuning Δ_s/γ at different temperatures, as shown in Fig. 2. It is sees

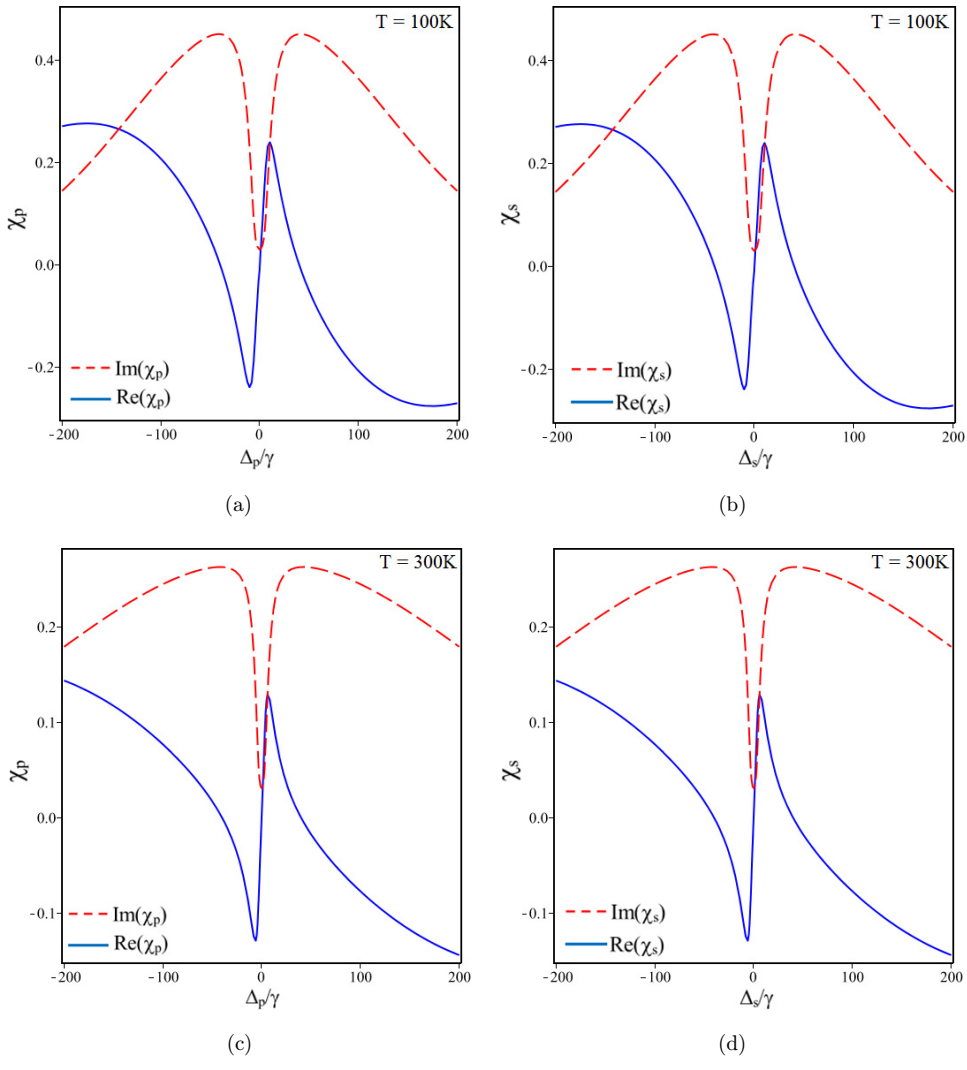

Fig. 2. Change of probe susceptibility χ_p versus probe detuning Δ_p/γ when $\Delta_c = \Delta_s = 0$ (a) and (c). Change of signal susceptibility χ_s versus signal detuning Δ_s/γ when $\Delta_c = \Delta_p = 0$ (b) and (d). Other used parameters are $\Omega_p = \Omega_s = 1\,\gamma$, $\Omega_c = 40\,\gamma$ and $T = 100\,\mathrm{K}$ for (a) and (b) and $T = 300\,\mathrm{K}$ for (c) and (d). The dashed and solid lines correspond to absorption and dispersion.

that: *first*, in the presence of strong coupling beam the EIT effect appears for both probe and signal fields. Correspondingly, normal dispersion curve are also present in the EIT window, so the group velocity will be manipulated at this frequency region; *second*, the depth and width of the EIT window decreases as the temperature increases and thus reduces the height of normal dispersive curve inside the EIT window; *third*, under two photon resonant condition or equal detunings, the position of the EIT window for the probe beam is identical to that for the signal beam.

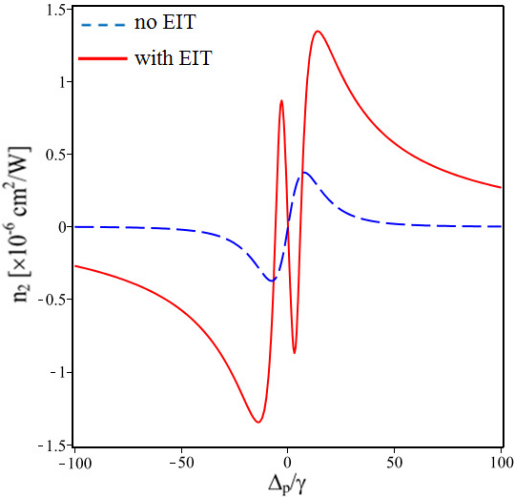

Fig. 3. Cross-Kerr nonlinear coefficient n_2 as a function of probe detuning when $\Omega_c = 0$ (dashed line), $\Omega_c = 40\,\gamma$ (solid line), $\Omega_p = \Omega_s = 1\,\gamma$, $\Delta_c = \Delta_s = 0$ and $T = 300\,\mathrm{K}$.

Therefore, the group velocity matching can also be realized and cross-Kerr nonlinearity is also enhanced as shows in Fig. 3.

In Fig. 3, we plot cross-Kerr nonlinearity n_2 for the probe beam with the respect to probe frequency detuning in two cases of the absence (dashed line) and the presence (solid line) of EIT effect as illustrated in Fig. 3. The parameters we have chosen for Fig. 3 are $\Omega_c = 0$ (dashed line), $\Omega_c = 40\,\gamma$ (solid line), $\Omega_p = \Omega_s = 1\,\gamma$, $\Delta_c = \Delta_s = 0$ and $T = 300\,\mathrm{K}$. From figure one can see that cross-Kerr nonlinearity is significantly enhanced around transparent spectral region at $\Delta_p = 0$. Namely, a nonlinear dispersive curve appears corresponding to the transparent spectral region and therefore there is a pair of positive–negative peaks of n_2 around $\Delta_p = 0$. Moreover, comparison between the two cases shows that cross-Kerr nonlinearity n_2 is enhanced by several orders of magnitude when the EIT presents. This phenomenon is similar to that of self-Kerr nonlinearity which experimentally demonstrated by Xiao *et al.*[13]

In order to see the influence of Doppler broadening on cross-Kerr nonlinearity, we plot n_2 versus probe detuning at different temperatures $T = 100\,\mathrm{K}$ (dashed line) and $T = 300\,\mathrm{K}$ (solid line) as displayed in Fig. 4. Other parameters used in Fig. 4 are $\Omega_c = 40\,\gamma$, $\Omega_p = \Omega_s = 1\,\gamma$ and $\Delta_c = \Delta_s = 0$. It is clear that the amplitude of the Kerr nonlinearity decreases as the temperature of atoms increases. This can be explained by the fact that the increase in temperature leads to a decrease in the atomic coherence and thus reduces the EIT efficiency we have seen in Fig. 2.

Finally, in Fig. 5, we fixed the parameters of laser beams at $\Delta_p = -5\gamma$, $\Delta_c = \Delta_s = 0$, $\Omega_c = 40\,\gamma$ and $\Omega_p = \Omega_s = 1\,\gamma$ which is corresponding to a positive peak of n_2 in Fig. 2, and plotted cross-Kerr nonlinear coefficient versus the temperature. Again shows that the maximum value of n_2 decreases as the temperature increases.

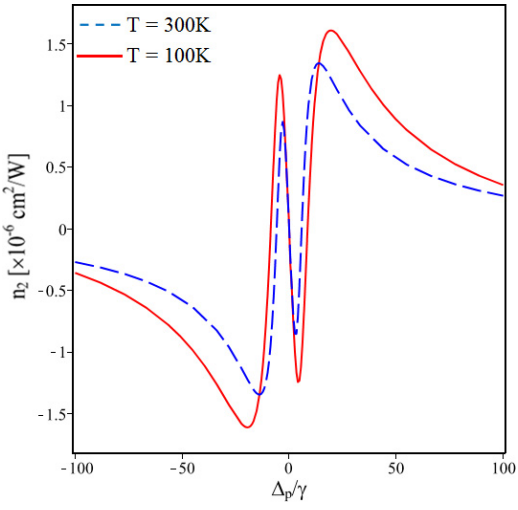

Fig. 4. Cross-Kerr nonlinear coefficient n_2 as a function of probe detuning at different temperatures $T = 100\,\mathrm{K}$ (dashed line) and $T = 300\,\mathrm{K}$ (solid line) when $\Omega_c = 40\,\gamma$ (solid line), $\Omega_p = \Omega_s = 1\,\gamma$, $\Delta_c = \Delta_s = 0$ and $T = 300\,\mathrm{K}$.

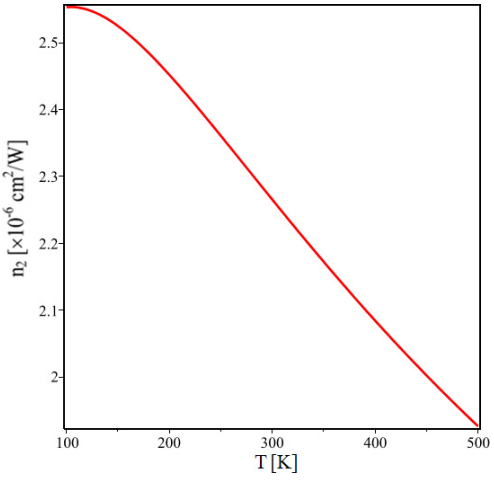

Fig. 5. Variation of Kerr-nonlinearity versus the temperature when $\Omega_c = 40\,\gamma$, $\Omega_p = \Omega_s = 1\,\gamma$, $\Delta_c = \Delta_s = 0$ and $\Delta_p = -5\,\gamma$.

For example, at temperature $T = 100\,\mathrm{K}$ the value of $n_2 = 2.55 \times 10^{-6}\,\mathrm{cm}^2/\mathrm{W}$, while at $T = 500\,\mathrm{K}$ the value of $n_2 = 1.92 \times 10^{-6}\,\mathrm{cm}^2/\mathrm{W}$.

4. Conclusion

We have studied the influence of Doppler broadening on cross-Kerr nonlinearity in four-level inverted-Y atomic medium under the EIT condition. The expressions for

the first- and third-susceptibilities and cross-Kerr nonlinear coefficient are found as a function of parameters of the light fields and the temperature of medium. It is shown that in the presence of strong coupling field the EIT effect appears for both fields. The position of the EIT window for the probe beam is identical to that for the signal beam. Therefore, the group velocity matching can also be realized and cross-Kerr nonlinearity is also enhanced greatly around transparent spectral region. The Doppler effect leads to a reduction in the transparent efficiency and thus reduces the amplitude of cross-Kerr nonlinear coefficient. The analytical result not only gives sufficient knowledge on cross-Kerr nonlinearity, but is also convenient to make direct comparisons with experiments and supports future studies related to cross-Kerr nonlinear effect under different temperature conditions. We also hope that a such cross-Kerr nonlinear coefficient will be measured directly similar to what was done for self-Kerr nonlinearity.

Acknowledgment

Financial supports from the Vietnam Ministry of Education and Training under grant code B2018-HHT-04 and Vietnam National Foundation for Science and Technology Development under grant code 103.03-2017.332 are acknowledged.

References

1. R. W. Boyd, *Nonlinear Optics* (Academic, San Diego, CA., 1992).
2. C. Ottaviani, D. Vitali, M. Artoni, F. Cataliotti and P. Tombesi, Polarization qubit phase gate in driven atomic media, *Phys. Rev. Lett.* **90** (2003) 197902.
3. S. Rebic, D. Vitali, C. Ottaviani, P. Tombesi, M. Artoni, F. Cataliotti and R. Corbalan, Polarization phase gate with a tripod atomic system, *Phys. Rev. A* **70** (2004) 032317.
4. W. J. Munro, K. Nemoto and T. P. Spiller, Weak nonlinearities: A new route to optical quantum computation, *New J. Phys.* **7** (2005) 137.
5. M. A. Nielsen and I. L. Chuang, *Quantum Computation and Quantum Information* (Cambridge University Press, Cambridge, 2000).
6. M. D. Lukin and A. Imamoglu, Nonlinear optics and quantum entanglement of ultraslow single photons, *Phys. Rev. Lett.* **84** (2000) 1419–1422.
7. K. Nemoto and W. J. Munro, Nearly deterministic linear optical controlled-NOT gate, *Phys. Rev. Lett.* **93** (2004) 250502.
8. Q. Lin and J. Li, Quantum control gates with weak cross-Kerr nonlinearity, *Phys. Rev. A* **79** (2009) 022301.
9. M. Fleischhauer, A. Imamoglu and J. P. Marangos, Electromagnetically induced transparency: Optics in coherent media, *Rev. Mod. Phys.* **77** (2005) 633–673.
10. H. Schmidt and A. Imamogdlu, Giant Kerr nonlinearities obtained by electromagnetically induced transparency, *Opt. Lett.* **21** (1996) 1936.
11. H. Kang and Y. Zhu, Observation of large Kerr nonlinearity at low light intensities, *Phys. Rev. Lett.* **91** (2003) 093601.
12. A. Joshi and M. Xiao, Phase gate with a four-level inverted-Y system, *Phys. Rev. A* **72** (2005) 062319.
13. H. Wang, D. Goorskey and M. Xiao, Enhanced Kerr nonlinearity via atomic coherence in a three-level atomic system, *Phys. Rev. Lett.* **87** (2001) 073601.

14. H. Chang, Y. Du, J. Yao, C. Xie and H. Wang, Observation of cross-phase shift in hot atoms with quantum coherence, *Europhys. Lett.* **65** (2004) 485.
15. Z.-B. Wang, K.-P. Marzlin and B. C. Sanders, Large cross- phase modulation between slow copropagating weak pulses in ^{87}Rb, *Phys. Rev. Lett.* **97** (2006) 063901.
16. X. D. Yang, S. J. Li, C. H. Zhang and H. Wang, Enhanced cross-Kerr nonlinearity via electromagnetically induced transparency in a four-level tripod atomic system, *J. Opt. Soc. Am. B* **26** (2009) 1423–1434.
17. J. Kou, R. G. Wan, Z. H. Kang, H. H. Wang, L. Jiang, X. J. Zhang, Y. Jiang and J. Y. Gao, EIT-assisted large cross-Kerr nonlinearity in a four-level inverted-Y atomic system, *Opt. Soc. Am. B* **27** (2010) 2035–2039.
18. C. Zhu and G. Huang, Giant Kerr nonlinearity, controlled entangled photons and polarization phase gates in coupled quantum-well structures, *Opt. Exp.* **19** (2011) 23364–23376.
19. D. X. Khoa, L. V. Doai, D. H. Son and N. H. Bang, Enhancement of self-Kerr nonlinearity via electromagnetically induced transparency in a five-level cascade system: An analytical approach, *J. Opt. Soc. Am. B.* **31**, (2014) 1330.
20. L. V. Doai, D. X. Khoa and N. H. Bang, EIT enhanced self-Kerr nonlinearity in the three-level lambda system under Doppler broadening, *Phys. Scr.* **90** (2015) 045502.
21. H. R. Hamedi, A. H. Gharamaleki and M. Sahrai, Colossal Kerr nonlinearity based on electromagnetically induced transparency in a five-level double-ladder atomic system, *App. Opt.* **55** (2016) 5892–5899.
22. L. T. M. Phuong, L. V. Doai, D. X. Khoa and N. H. Bang, Optical bistability in a controllable giant self-Kerr nonlinear gaseous medium under electromagnetically induced transparency and Doppler broadening, *Inter. J. Opt.* **2018** (2018) 1–7.
23. D. A. Steck, Rb^{87} D Line Data, http://steck.us/alkalidata.